PHYSICAL REVIEW B VOLUME 48, NUMBER 3 15 JULY 1993-I

Theoretical study on the electronic structure of $(Si)_m/(Ge)_n$ superlattices

M. Ikeda
Fujitsu Laboratories Ltd., 10-1, Morinosato-Wakamiya, Atsugi-shi, Kanagawa 243-01, Japan

K. Terakura
Institute for Solid State Physics, University of Tokyo, Roppongi, Minato-ku, Tokyo 106, Japan

T. Oguchi
National Research Institute for Metals, Nakameguro, Meguro-ku, Tokyo 153, Japan
(Received 14 January 1993)

The electronic structures of $(Si)_m/(Ge)_n$ superlattices with (001) stacking were studied by using the linear-muffin-tin-orbital method. A simple scheme of a self-interaction correction was implemented in order to predict the semiconductor band gap quantitatively. As the ten-layer periodicity is particularly suitable for realizing direct-band-gap superlattices, we studied several modulated superlattices $(Si)_{m'}/(Ge)_{n'}/(Si)_{m''}/(Ge)_{n''}\cdots$ with $m'+n'+m''+n''+\cdots=10$. We found interesting variations in the symmetry of the conduction-band bottom state and also in the wave-function confinement in the Si layer with regard to the variation in the set of $(m',n',m'',n'',\ldots)$. These results were analyzed with simple models. The dipole transition probability was also estimated. Some calculations were also performed to discuss the alloying effects at the interface for the $(Si)_4/(Ge)_4$ superlattice on the Si substrate.

I. INTRODUCTION

Recent progress in the technique of crystal growth has made it possible to create atomic-layer-controlled strained semiconductor superlattices, which are designed to exhibit desired properties in transport and optical phenomena. For example, ultrathin $(Si)_m/(Ge)_n$ superlattices have been grown on the (001)Si and SiGe alloy substrates,[1-4] with an aim of creating direct-band-gap materials from originally indirect-band-gap materials.[5] New low-energy optical transitions were observed for the $(Si)_4/(Ge)_4$ superlattice grown on the Si substrate[1] and photoluminescence with 0.85 eV was observed for the $(Si)_6/(Ge)_4$ superlattice grown on the SiGe alloy substrate.[3] These experimental facts may be taken as indications of realization of direct-band-gap materials.[4] However, in order to determine the band-gap character definitely, supplementary information from the first-principles electronic structure calculations is indispensable. Several band-structure calculations have, in fact, been performed for Si-Ge superlattices.[6-13] Nevertheless, there still exist some discrepancies between theoretical and experimental results. Further theoretical studies are therefore needed. Another important aspect of theoretical study is to predict new interesting phenomena by studying various types of superlattices which may or may not be accessible by the present experimental technique. Here we would like to add some contributions to the existing theoretical works.

The present band-structure calculations were performed with the linear-muffin-tin-orbital (LMTO) method[14] and based on the local-density approximations (LDA) in the density-functional theory.[15] Empty spheres were introduced and the combined correction was implemented.[14] Unlike the usual use of $\kappa^2=0$, we adopted a small negative κ^2 in order to deal with the Γ point unambiguously, which is crucially important for the present purpose. In order to correct the LDA for the underestimation of band gaps, we adopted a simple version of the self-interaction correction (SIC).[11,16]

In a previous work,[17] we found that the symmetry of the wave function of the lowest and the second-lowest conduction-band states of the $(Si)_{2m}/(Ge)_{10-2m}$ superlattice on the Ge and the SiGe alloy substrate alternates between Γ_1^+ and Γ_3^- as m increases from 1 to 4. This symmetry alternation is important because the optical transition from the valence-band top to the conduction-band bottom is allowed (forbidden) if the lowest conduction-band state has Γ_3^- (Γ_1^+) symmetry. In the present work, we found that such symmetry alternation occurs in more general modulated superlattices $(Si)_{m'}/(Ge)_{n'}/(Si)_{m''}/(Ge)_{n''}\cdots$ with $m'+n'+m''+n''+\cdots=10$. The first-order perturbation theory presented in the previous paper[17] also works in the general cases. Charge-density analysis provides a reasoning of the success of such a simple theory. We also observe an interesting trend in the wave-function confinement of the lowest and the second-lowest conduction-band states within the Si layer for the general modulated superlattices. Although we have not completely understood the mechanism of this phenomenon, we demonstrate that a similar phenomenon can also occur in simple one-dimensional models. It is also important to note that a proper tuning of the set $(m',n',m'',n'',\ldots)$ for the modulated superlattices can adjust the band-gap and more importantly maximize the optical transition probability, which is an important factor for photoemitter.

One of the most important discrepancies between theory and experiment is that the experimentally observed 0.76-eV transition for the $(Si)_4/(Ge)_4$ superlattice

 ©1993 The American Physical Society

on the Si substrate[1,18,19] cannot be explained consistently.[12,19] Theoretical studies have always assumed an ideally sharp interface, while real superlattices have interdiffused interfaces. We studied effects of alloying at the interface for the above-mentioned superlattice. Within our model study, the discrepancy between theory and experiment cannot totally be removed. Nevertheless, the alloying effect can partially resolve the problem. We also point out that partial relaxation of strain in the superlattice may also reduce the discrepancy.

In Sec. II, some details of the methodological aspect will be described. Calculated results and their analysis will be presented in Sec. III. Concluding remarks will be made in Sec. IV.

II. METHODOLOGY

The lattice constant of Ge is 4% larger than that of Si. The Si or Ge atoms in the superlattices are expanded or compressed due to the strain caused by the substrate. The distance between the adjacent plane is determined by the valence force field (VFF) method.[20]

As an all-electron band calculation technique, we have employed the LMTO method with the atomic-sphere approximation (ASA).[14] The combined corrections and the empty spheres are incorporated. The orbitals are determined via the scalar relativistic equation and the core states are relaxed in every iteration step. In order to avoid the divergence of the structure constant and the combined corrections occurring at the Γ point in the conventional LMTO method with the energy parameter κ being zero, we have employed a small imaginary κ. This enables us to discuss the energy eigenvalues and the transition probabilities just at the Γ point unambiguously.

In the present work, the electronic structure calculations are performed within the LDA in the density-functional theory.[15] Although the ground-state properties of condensed matters are well described by the LDA, the band gap of semiconductors is significantly underestimated. In order to circumvent this situation, we have implemented SIC into the LMTO method.[11] In our method, which is similar to one of the versions of Hamada and Ohnishi,[16] the SIC is considered only for the p states because the wave function of the valence-band top is composed mainly of the p states. The SIC is incorporated in the basis orbital defined by

$$[H^{\mathrm{LDA}}(\mathbf{r})+\delta_{l1}V_{il}^{\mathrm{SIC}}(\mathbf{r})]\Psi_{il}(\mathbf{r})=E_{il}\Psi_{il}(\mathbf{r}) , \quad (1)$$

where i specifies atomic species, δ_{l1} is the Kronecker delta, and the SIC potential V_{il}^{SIC} is given by

$$V_{il}^{\mathrm{SIC}}(\mathbf{r})=-f_{il}\left[V_{\mathrm{xc}}(\rho_{il},0)+\int d^3r'\frac{\rho_{il}(\mathbf{r}')}{|\mathbf{r}-\mathbf{r}'|}\right] , \quad (2)$$

$$f_{il}=\int_{-\infty}^{E_F}D_l(E)dE/(2l+1) . \quad (3)$$

In the above equations, f_{il} is an effective occupation number, $\rho_{il}(\mathbf{r})$ is the electron density for the partial wave specified by (i,l), and V_{xc} is the exchange-correlation potential. In our treatment, the SIC affects the band structure through the potential parameters of the p orbitals. The top of the valence bands is moved downwards due to subtraction of the self-interaction, whereas the bottom of the conduction bands is scarcely affected. Thereby the energy gap of the semiconductors becomes larger.

III. RESULTS AND DISCUSSION

A. Atomic structure, band gap, and band offset

First we summarize some results for fundamental aspects of the present problem. As mentioned above, the atomic structure was optimized by the VFF method. The bond length between Si and Ge is estimated to be 2.38 Å in $(\mathrm{Si})_5/(\mathrm{Ge})_5$ grown on a Si substrate, being in good agreement with the experimental value 2.37 Å obtained by surface extended x-ray-absorption fine structure (EXAFS).[21] The distance between adjacent atomic planes is illustrated in Fig. 1 for $(\mathrm{Si})_6/(\mathrm{Ge})_4$ grown on both a SiGe alloyed substrate and a Ge substrate. The result is quite close to other calculations.[6,13] The heterointerface distance is approximately equal to an arithmetic average of the Si-Si and Ge-Ge atomic plane distances.

The band gaps obtained by the present SIC-LMTO-ASA method are summarized in Table I for some semiconductors. The calculated values agree fairly well with experiment even for III-V compound semiconductors. This will allow us to argue the absolute value of the band gap for the Si-Ge superlattice within an accuracy of about 0.1 eV. There is one rather inconvenient aspect for Ge in our calculation: the conduction-band bottom at the Γ point is higher in energy than that at the L point only by 0.027 eV, while the experimental energy difference is 0.154 eV. However, this will not affect the main part of the following arguments because the band gap in the Si-Ge superlattice comes from the states of mostly Si origin, which are originally along the Δ line and are folded to the Γ point. In order to provide information about the quality of the present calculation in a wider energy range, we summarize in Table II the energy levels at the high-symmetry points for Si as an example obtained by the LDA-LMTO-ASA, the SIC-LMTO-ASA,

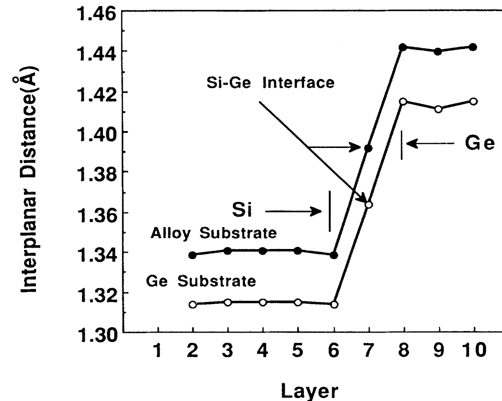

FIG. 1. The interplanar distances between the adjacent atomic planes in the strained layer $(\mathrm{Si})_6/(\mathrm{Ge})_4$ superlattice determined by the valence-force-field method for both the SiGe alloy and the Ge substrate.

TABLE I. The experimental and the present theoretical values of the band-gap energy in eV for the typical semiconductors.

Semiconductors	Experiment	Present theory	Transition type
Si	1.17	1.19	$\Gamma-\Delta$
Ge	0.74	0.75	$\Gamma-L$
GaAs	1.52	1.66	$\Gamma-\Gamma$
AlAs	2.23	2.42	$\Gamma-X$

the *GW* approximation based on the FLAPW (full-potential linear-augmented-plane-wave) method,[22] and the experiment.[23,24] As the present SIC calculation lowers the valence-band top, the total valence-band width is underestimated by an appreciable amount. On the other hand, the conduction-band energies agree fairly well with experiment.

The band offset can also be estimated from our band-structure calculations for $(Si)_5/(Ge)_5$ in the following way. We followed the procedure adopted by an experimental analysis,[25,26] while a different approach was adopted by Van de Walle and Martin.[27] Let us explain the present procedure by taking the Ge substrate case (the left one in Fig. 2) as an example. By using the energy levels of Si and Ge at each center of the Si and Ge layers, the energy difference between the Ge 3*d* state and the Si 2*p* state is estimated to be 65.667 eV. Assuming that the electronic structures at each central layer are identical to those in the corresponding bulk material, we estimate the energy difference between the 2*p* level and the valence-band top in the tetragonally strained Si and also the one between the 3*d* level and the valence-band top in the strain-free bulk Ge. The obtained values are 88.901 and 23.432 eV, respectively. Arranging these levels in the way as shown

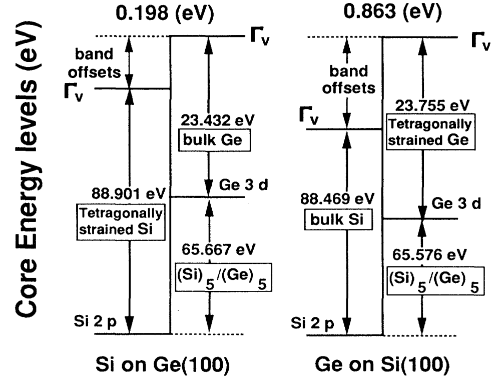

FIG. 2. The energy-level diagrams for Si on Ge(001) and for Ge on Si(001) are shown by using the scheme of Refs. 25 and 26. The core energy levels are determined at the middle layer of the $(Si)_5/(Ge)_5$ superlattices.

in the left diagram of Fig. 2, we obtain 0.198 eV as the band offset for the Ge substrate case. This agrees well with the observed value of 0.17 ± 0.13 eV.[25] Similarly, the band offset for Ge on the Si(001) substrate is 0.863 eV from our calculation and 0.74 ± 0.13 eV from experiment.[25]

As the top of the Ge valence band is located higher in energy than that of Si, valence electrons flow from the Ge layer to the Si layer to some extent. Figure 3 shows the net charge distribution of $(Si)_{2m}/(Ge)_{10-2m}$ ($m=1$, 2, 3, and 4) grown on the Ge substrate. The vertical value at each node denotes the net charge per atom of each layer which is composed of the nuclear charge and the electron charge including the contribution from the empty spheres. A negative value means an increased number of electrons.

TABLE II. The experimental and the theoretical energy levels in eV at the high-symmetry points for silicon.

High-symmetry points	Present calculations (LDA-LMTO)	Present calculations (SIC-LMTO)	*GW* approx. (FLAPW)[a]	Expt.[b]
Γ_{1v}	−12.06	−11.12	−12.21	−12.5
$\Gamma_{25'v}$	0.00	0.00	0.00	0.00
$\Gamma_{15'c}$	2.66	2.94	3.30	3.34
$\Gamma_{2'c}$	3.13	4.12	4.19	4.15
X_{1v}	−7.92	−7.20	−8.11	
X_{4v}	−2.91	−2.87	−3.03	−2.9
X_{1c}	0.59	1.36	1.14	1.3[c]
$L_{2'v}$	−9.73	−8.84	−9.92	−9.3
L_{1v}	−7.12	−6.65	−7.31	−6.8
$L_{3'v}$	−1.17	−1.20	−1.26	−1.2
L_{1c}	1.38	2.25	2.15	2.04
L_{3c}	3.24	3.76	4.08	3.9

[a]Reference 22.
[b]Reference 23, except where noted.
[c]Reference 24.

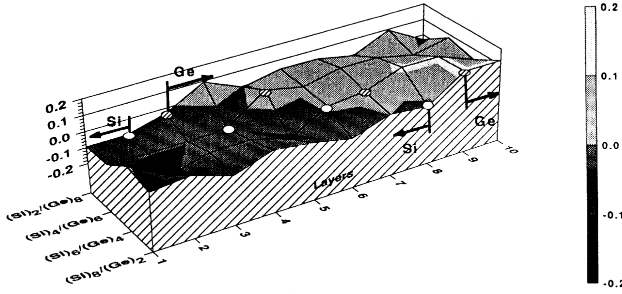

FIG. 3. The net charge distribution in $(Si)_{2m}/(Ge)_{10-2m}$ ($m=1$, 2, 3, and 4) grown on the Ge substrate. The vertical value at each node denotes the net charge per atom of each layer. The node at the interface of the Si (Ge) layer is indicated by the open circle (shaded circle). The valence electrons flow from the Ge layer to the Si layer. A negative value means an increased number of electrons.

B. $(Si)_{2m}/(Ge)_{10-2m}$ ($m=1$, 2, 3, and 4): Periodic alternation of allowed and forbidden transitions

With a simple zone-folding scheme, it is understandable that a periodicity of ten-layer thickness is particularly suitable for making the Si/Ge system a direct-gap semiconductor. In the present calculation, in fact, $(Si)_{2m}/(Ge)_{10-2m}$ is of direct-gap type for all m from 1 to 4 when it is grown on either a Ge or SiGe alloy substrate whose composition is the same as the superlattice. (In the case of the Si substrate, the conduction-band minimum is located along the Δ line parallel to the stacking plane.) The present results for the energy gap are summarized in Table III. For $(Si)_6/(Ge)_4$ on the SiGe alloy substrate, an experimental value of 0.85 eV is rather close to the present estimation of 0.664 eV. In Table III, "pseudodirect" means that the lowest optical transition between the conduction and valence bands is forbidden, while it is allowed for "direct."

In Fig. 4, the band dispersion of $(Si)_2/(Ge)_8$ grown on a Ge substrate is shown as a typical example. The dispersion curves are plotted by using the original fcc lattice Brillouin zone. This $E-\mathbf{k}$ curve clearly shows that the conduction-band minimum is located at the Γ point. In order for the system to be useful as a photoemitter, it is also crucial that the lowest-energy direct optical transition is allowed. However, in several cases, this criterion is not satisfied although the system is of the direct-gap type. Recently, we showed theoretically that the symmetry of the wave function of the lowest and the second-lowest conduction-band states at the Γ point alternates between Γ_1^+ and Γ_3^- as m increases from 1 to 4.[17] Therefore, the lowest-energy optical transition is forbidden for $m=2,4$ and allowed for $m=1,3$ as shown in Table II, where the energy difference $\Delta E[\equiv E(\Gamma_3^-)-E(\Gamma_1^+)]$ is also shown. The energy diagrams at the Γ point for the Ge and the SiGe alloy substrate cases are shown in Fig. 5, where the optical dipole transition is allowed between levels connected by a vertical arrow.

In a previous paper, by adopting the first-order perturbation theory for the pseudopotentials of Si and Ge, we have analyzed the alternation of Γ_1^+ and Γ_3^- symmetries for the lowest and the second-lowest states. We gave the following simple expression for the energy difference:

$$\Delta E = E(\Gamma_3^-)-E(\Gamma_1^+) = \frac{4}{5}\sum_{n=1}^{5}(-1)^n \sin\left[\frac{4\pi z_n}{5a\xi}\right] \times V_n\left[\frac{2\sqrt{2}\pi}{a},\frac{2\sqrt{2}\pi}{a},\frac{4\pi}{5a\xi}\right], \quad (4)$$

where the summation is taken over the layers with index n as indicated in Fig. 6 and z_n is the position of the nth layer. $V_n[k_x,k_y,k_z]$ is a Fourier component of the pseudopotential $V_n(r)$ of the atom in the nth layer. Assuming equal interlayer spacing and noting that V_n can be replaced by $\Delta V_n = V_n - V_{Ge}$, we can reduce ΔE of Eq. (4) to

TABLE III. The energy difference $\Delta E[=E(\Gamma_3^-)-E(\Gamma_1^+)]$ between the lowest two conduction-band states and the energy gap are shown for the $(Si)_{2m}/(Ge)_{10-2m}$ superlattices with $m=1$, 2, 3, and 4 on the Ge and the SiGe alloy substrates. $(\Delta E)_{LMTO}$ is derived from our SIC-LMTO calculations, while $(\Delta E)_{PT}$ is estimated by the first-order perturbation theory. As for the transition type, "pseudodirect" means that the lowest optical transition is forbidden, while it is allowed for "direct."

$(Si)_m/(Ge)_{10-m}$	$m=2$	$m=4$	$m=6$	$m=8$
Ge substrate				
$(\Delta E)_{LMTO}$	−0.270	0.088	−0.101	0.024
$(\Delta E)_{PT}$	−0.042	0.070	−0.071	0.044
Energy gap (eV)	0.739	0.708	0.664(0.85[a])	0.623
Transition type	Direct	Pseudodirect	Direct	Pseudodirect
SiGe substrate				
$(\Delta E)_{LMTO}$	−0.279	0.092	−0.099	0.028
$(\Delta E)_{PT}$	−0.043	0.070	−0.071	0.045
Energy gap (eV)	0.786	0.885	1.01	1.15
Transition type	Direct	Pseudodirect	Direct	Pseudodirect

[a]Experimental value from Ref. 3.

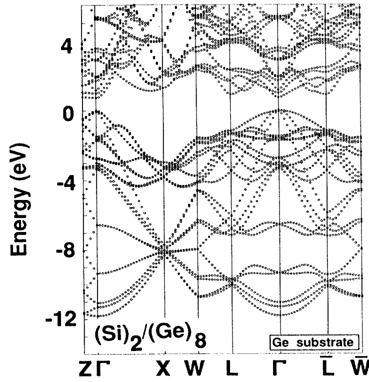

FIG. 4. The $E-\mathbf{k}$ curves of the strained layer $(\mathrm{Si})_2/(\mathrm{Ge})_8$ superlattice grown on the Ge substrate. The energy curves are plotted in the original fcc Brillouin zone. As the symmetry of the point group of superlattices is lower than the original fcc lattice, there appear inequivalent high-symmetry points. L, $\bar{L}$, W, and $\bar{W}$ are such examples. In the superlattice Brillouin zone (bct), the L (W) point is not connected to the $\bar{L}$($\bar{W}$) point under the operation of D_{2h}.

$$\Delta E\,[(\mathrm{Si})_{2m}/(\mathrm{Ge})_{10-2m}]$$

$$=(-1)^m\frac{2}{5}\frac{\sin(m/5)\pi}{\cos(\pi/10)}\Delta V\left[\frac{2\sqrt{2}\pi}{a},\frac{2\sqrt{2}\pi}{a},\frac{4\pi}{5a\xi}\right], \tag{5}$$

where $\Delta V=V_{\mathrm{Si}}-V_{\mathrm{Ge}}$. We estimated ΔV by the analytic expression given by Friedel, Hybertsen, and Schlüter[28] and demonstrated that Eq. (5) explains the alternating sign change in Fig. 5. ΔE by Eq. (5) is shown in Table III as $(\Delta E)_{\mathrm{PT}}$.

Let us study the reason why the present simple analysis can account well for the alternation of Γ_1^+ and Γ_3^- symmetries. It should be noted that ΔE is determined by the quantity

$$\delta|\phi(\mathbf{r})|^2=\{|\phi(\mathbf{r}:\Gamma_3^-)|^2-|\phi(\mathbf{r}:\Gamma_1^+)|^2\},$$

where $\phi(\mathbf{r}:\Gamma_i)$ is the wave function of the Γ_i symmetry. With $\phi(\mathbf{r}:\Gamma_i)$ given by Eqs. (3) and (4) of Ref. 17, $\delta|\phi(\mathbf{r})|^2$ is illustrated in the upper part of Fig. 7 within each atomic plane shown in Fig. 6. Contours for positive (negative) $\delta|\phi(\mathbf{r})|^2$ denoted by solid (dashed) curves and $\delta|\phi(\mathbf{r})|^2$ vanishes along the dotted curves. In the lower part of Fig. 7, the atomic position in each atomic plane is denoted by open circles, to which ΔV_n is associated for estimating ΔE. For $m=1$, $\Delta V_1=\Delta V=V_{\mathrm{Si}}-V_{\mathrm{Ge}}$ and all other ΔV_n's are zero. As $\delta|\phi(\mathbf{r})|^2$ is negative at the atomic position for $n=1$ and ΔV_1 is positive, ΔE is negative. For $m=2$, we have to add a contribution from the $n=2$ atomic plane to ΔE for $m=1$. In the $n=2$ atomic plane, $\delta|\phi(\mathbf{r})|^2$ is strongly positive at the atomic position and therefore the positive contribution overwhelms the negative ΔE from the $n=1$ atomic plane. We can proceed similarly for larger m's. We claimed in a previous paper that the $\delta|\phi(\mathbf{r})|^2$ in the perturbation theory would be a good approximation for the corresponding one obtained by the band-structure calculation. Figure 8 shows $\delta|\phi(\mathbf{r})|^2$'s obtained for $(\mathrm{Si})_{2m}/(\mathrm{Ge})_{10-2m}$ for all $m=1$–4. Clearly, the essential aspect of Fig. 7 discussed in the preceding paragraph can also be seen in Fig. 8 except for a somewhat qualitative difference in the case of $m=1$. This is due to a fairly strong wave-function confinement in the Si layer for $m=1$,[17] which is not taken into consideration in the perturbative treatment. A large discrepancy in ΔE between the band calculation and the perturbation theory can also be seen for $m=1$ as shown in Table III.

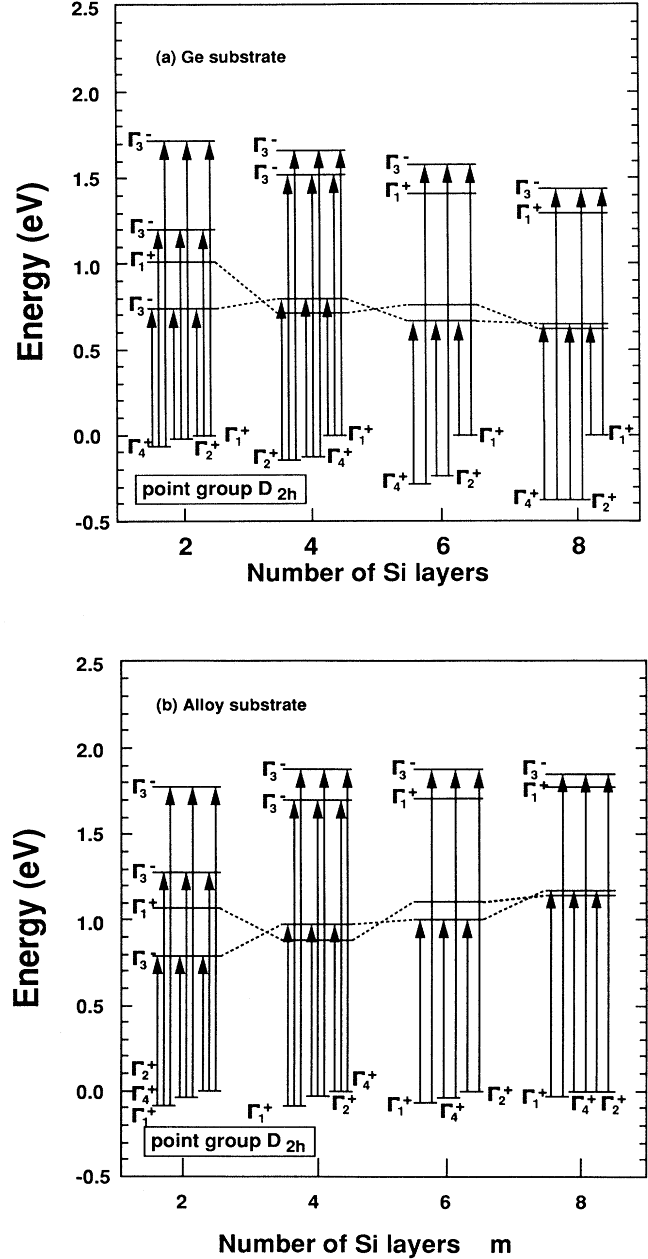

FIG. 5. Energy-level diagrams at the Γ point for $(\mathrm{Si})_{2m}/(\mathrm{Ge})_{10-2m}$ (a) on the Ge(001) substrate, (b) on the SiGe alloy substrate. The lowest three levels belong to the valence band and the higher four levels to the conduction band. Optical transition is allowed between states connected by an arrow.

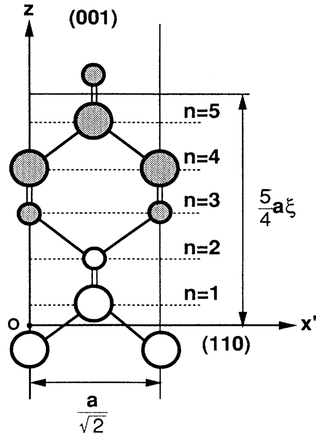

FIG. 6. Projection of atomic position in the $(Si)_4/(Ge)_6$ superlattice onto a zx' plane. The x' axis is along the [110] direction and y' axis the $[\bar{1}10]$ direction of the original diamond lattice. Shaded (open) circles denote Ge (Si). The larger circles denote atoms in the $y'=0$ plane and the smaller ones those in the $y'=(\sqrt{2}/4)a$ plane. The origin of the coordinate system is denoted by O.

For an application of these superlattices as photoemitter, the optical transition probability is an important problem. In Table IV, we show the allowed transition energy levels at the Γ point and the calculated values of the dipole matrix element squared which are normalized by the lowest-energy bulklike transition. Γ_{ci} (Γ_{vi}) denotes the ith conduction- (valence-) band level. The photon polarization associated with each transition is also indicated as P_x or P_y or P_z. The results in Table IV are for the SiGe alloy substrate. Similar calculations were performed also for the Ge substrate, though we do not present the results. We found that the substrate dependence of the polarization for the lowest-energy transition reflects the substrate dependence of the energy level ordering at the valence-band top.

C. Modulated superlattices

As mentioned before, the ten-layer periodicity is a suitable condition for realizing a direct band gap. A further interesting aspect of artificial superlattices is that it may be possible to introduce finer modulations to the superlattice within a given periodicity. Let us consider a case $(Si)_{m'}/(Ge)_{n'}/(Si)_{m''}/(Ge)_{n''}\cdots$ with $m=m'+m''+\cdots$, $n=n'+n''+\cdots$, and $m+n=10$. Hereafter a simplified notation $(m'/n'/m''/n''/\cdots)$ will also be used to denote the above-modulated superlattice. In addition to the variation of m (or n), it is also possible to tune the band gap and to maximize the transition probability by choosing the set $(m',m'',\ldots)$ and $(n',n',\ldots)$ properly. In this subsection, we discuss some of such variations with the Ge substrate. $(Si)_m/(Ge)_{5-m}$ ($m=1-4$) has a five-layer periodicity with regard to the composition modulation. However, to be compatible with the four-layer periodicity of the diamond lattice, it forms a body-centered tetragonal lattice with the same c-axis periodicity as the ten-layer periodicity case. However, the symmetry at the Γ point is D_{4h}. We performed band-structure calculations for $(Si)_2/(Ge)_3$ and $(Si)_3/(Ge)_2$, for both of which the conduction-band minimum is located at the Γ point. The symmetries of the lowest two states of the conduction band at the Γ point are again Γ_1^+ and Γ_2^- and their ordering alternates between $(Si)_2/(Ge)_3$ and $(Si)_3/(Ge)_2$. Note that the Γ_2^- symmetry in D_{4h} corresponds to the Γ_3^- symmetry in D_{2h}.[29] The Γ_1^+ state is lower (higher) than the Γ_2^- state for $(Si)_3/(Ge)_2$[$(Si)_2/(Ge)_3$]. As shown in Fig. 9, the dipole transition is allowed between the Γ_2^- state and the doubly degenerate Γ_5^+ states of the valence band. In the case of the SiGe alloy substrate, the ordering of the Γ_3^+ and Γ_5^+ states of the valence band is reversed. The (2/2/3/3) superlattice has a C_{2v} symmetry at the Γ point. In this case, although the dipole transition is allowed between the valence-band states and the lowest conduction-band state whose symmetry is Γ_1, the conduction-band minimum is slightly off the Γ point. For (2/2/4/2) and (2/2/2/4) superlattices, the conduction-band minimum is located at the Γ point whose symmetry is D_{2h}. The energy gaps for (2/2/4/2) and (2/2/2/4) are 0.71 and 0.81 eV, respectively. As the energy gaps for $(Si)_6/(Ge)_4$ and $(Si)_4/(Ge)_6$ are 0.66 and 0.71 eV, respectively, the modulated structure has an effect of increasing the energy gap. The energy-level scheme at the Γ point is shown in Fig. 10, where we see again the alternation of the Γ_1^+ and Γ_3^- states at the conduction-band bottom.

As Eq. (4) is applicable to both the D_{4h} and D_{2h} cases,

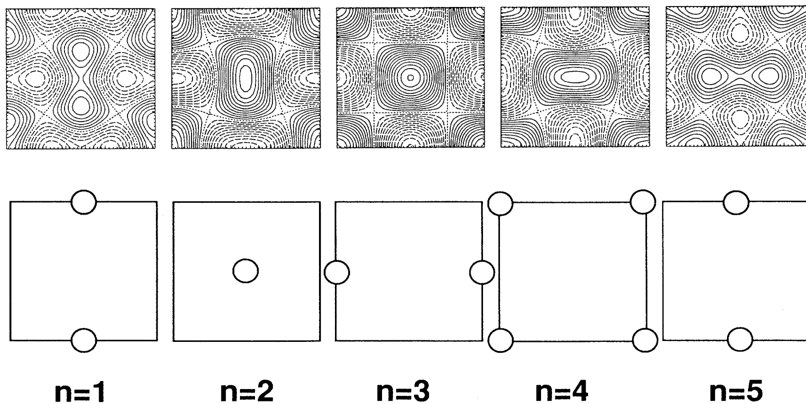

FIG. 7. Contour maps of the quantity $\delta|\phi(\mathbf{r})|^2=\{|\phi(\mathbf{r}:\Gamma_3^-)|^2-|\phi(\mathbf{r}:\Gamma_1^+)|^2\}$ obtained by the first-order perturbation theory are shown within each atomic plane as shown in Fig. 6. Contour for positive (negative) $\delta|\phi(\mathbf{r})|^2$ is denoted by solid (dashed) curves and $\delta|\phi(\mathbf{r})|^2$ vanishes along the dotted curves. In the lower part of this figure, the atomic position in each atomic plane is denoted by open circles.

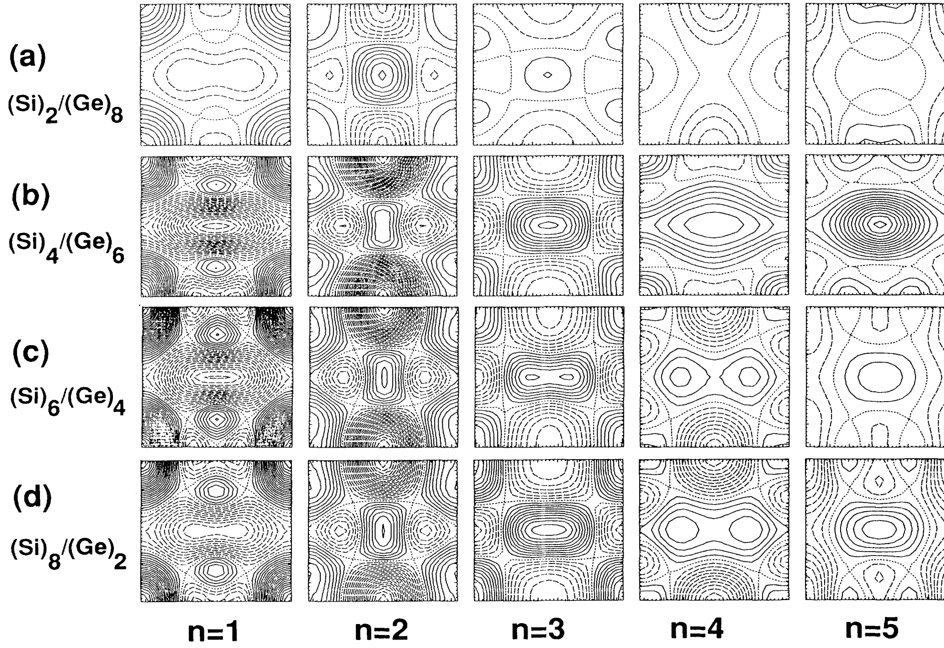

FIG. 8. The $\delta|\phi(\mathbf{r})|^2$'s obtained from the band-structure calculations for $(\mathrm{Si})_{2m}/(\mathrm{Ge})_{10-2m}$ for all $m=1$–4. For other aspects, the same as in Fig. 7.

the symmetry alternation in this subsection can also be analyzed with this simple expression. [Γ_3^- of Eq. (4) should be Γ_2^- for D_{4h}.] The estimated energy separations $E(\Gamma_3^-)-E(\Gamma_1^+)$ are summarized in Table V. The values in the parentheses are for $(\mathrm{Si})_{2m}/(\mathrm{Ge})_{10-2m}$. Even with the same composition, the magnitude and sign of $E(\Gamma_3^-)-E(\Gamma_1^+)$ change with the modulation and the first-order perturbation theory accounts well for the trend.

As a photoemitter, the dipole transition probability is a very important factor. Here we only point out that the dipole transition probability for the lowest transition for (2/2/2/4) is 2.98×10^{-2}. The corresponding transition for $(\mathrm{Si})_4/(\mathrm{Ge})_6$ is forbidden and that for $(\mathrm{Si})_6/(\mathrm{Ge})_4$ is only 1.1×10^{-3}. Therefore, the present study suggests that suitable modulated structures can enlarge the usefulness of superlattices in the application field. The wave function has some interesting behaviors in the modulated su-

TABLE IV. Calculated dipole matrix elements $|\langle i|P|f\rangle|^2$ and transition energies ΔE in $(\mathrm{Si})_{2m}/(\mathrm{Ge})_{10-2m}$ superlattices on the SiGe alloy (001) substrate. Energy differences are in eV. $\langle i|$ is a valence-band and $|f\rangle$ a conduction-band state. The direction of polarization is denoted by P_x, P_y, or P_z. The matrix elements are normalized by the lowest-energy bulklike transition.

	$\langle i\|$		Γ_{v_1}				Γ_{v_2}				Γ_{v_3}	
Type	$\|f\rangle$	ΔE	$\|\langle i\|P\|f\rangle\|^2$			ΔE	$\|\langle i\|P\|f\rangle\|^2$			ΔE	$\|\langle i\|P\|f\rangle\|^2$	
$m=1$	Γ_{c_1}	0.786	0.036	P_x		0.828	0.050	P_y		0.871	0.033	P_z
	Γ_{c_3}	1.27	1.0			1.316	1.0			1.36	1.0	
$m=2$	Γ_{c_2}	0.977	0.027	P_y		1.00	0.021	P_x		1.07	0.034	P_z
	Γ_{c_3}	1.70	0.334			1.73	0.211			1.79	0.307	
	Γ_{c_4}	1.88	1.0			1.91	1.0			1.97	1.0	
$m=3$	Γ_{c_1}	1.01	0.002	P_x		1.05	0.006	P_y		1.08	0.002	P_z
	Γ_{c_4}	1.88	0.021			1.92	0.087			1.95	0.029	
	Γ_{c_5}	1.97	0.020			2.01	0.008			2.04	0.016	
	Γ_{c_7}	2.46	1.0			2.50	1.0			2.53	1.0	
$m=4$	Γ_{c_2}	1.18	0.002	P_x		1.18	0.009	P_y		1.20	0.004	P_z
	Γ_{c_4}	1.85	0.002			1.85	0.019			1.88	0.001	
	Γ_{c_6}	2.17	0.03			2.17	0.051			2.20	0.023	
	Γ_{c_7}	2.92	1.0		Γ_{c_8}	2.93	1.0		Γ_{c_7}	2.95	1.0	

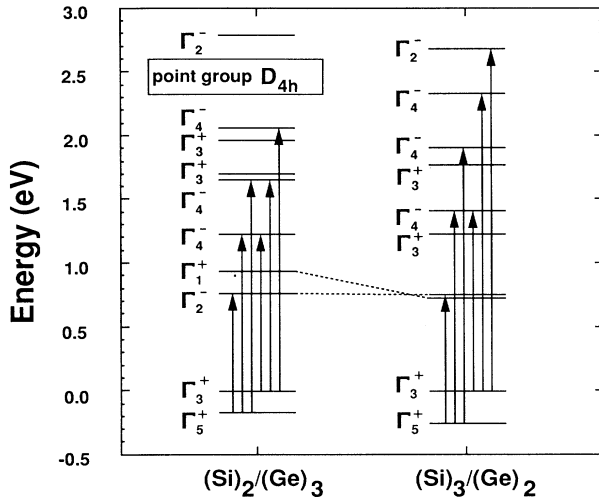

FIG. 9. Energy-level diagrams at the Γ point for $(Si)_m/(Ge)_{5-m}$ on the Ge(001) substrate. The symmetry at the Γ point is D_{4h}. Optical transition is allowed between states connected by an arrow. Γ_2^- of D_{4h} corresponds to Γ_3^- of D_{2h}.

perlattices. The integral of the wave function squared over the Si (Ge) atomic spheres in a unit cell, $\langle |\psi_i(\mathbf{r})|^2 \rangle_\nu$ [ν=Si (Ge)], is shown in Fig. 11(a) for (2/2/2/4) and (2/2/4/2). The solid (open) circles are for the lowest (second-lowest) conduction-band state at the Γ point. Along the abscissa, 4′ and 6′ denote the former and latter sublattices, respectively. The result for $(Si)_{2m}/(Ge)_{10-2m}$ in a previous paper is also shown as Fig. 11(b) for comparison. As Si has effectively a deeper potential than Ge, a stronger confinement of wave function within the Si atomic spheres for the lowest-energy state seems to be reasonable. However, this expectation is not necessarily correct as the Si layer becomes thicker as shown in Fig. 11(b). Further complication is found in Fig. 11(a) where the trend in Fig. 11(b) from $m=4$ to 6 is reversed for 4′ and 6′. At present, we have not completely understood the behavior of $\langle |\psi_i(\mathbf{r})|^2 \rangle_\nu$. Nevertheless, we would like to point out a similar behavior in a simple one-dimensional model. In Fig. 12, deeper potential regions correspond to Si layers and shallower potential regions to Ge layers. Figures 12(a)–12(d) simulate (2/8), (8/2), (2/2/2/4), and (2/2/4/2), respectively. In simple one-dimensional models, we consider the lowest two states at the Γ point, i.e., $k=0$. The vertical dot-dashed lines denote the positions with regard to which the system has mirror symmetry. The lowest state wave function (solid line) is symmetric, while the second-lowest state (dashed line) is antisymmetric with regard to mirror symmetry.

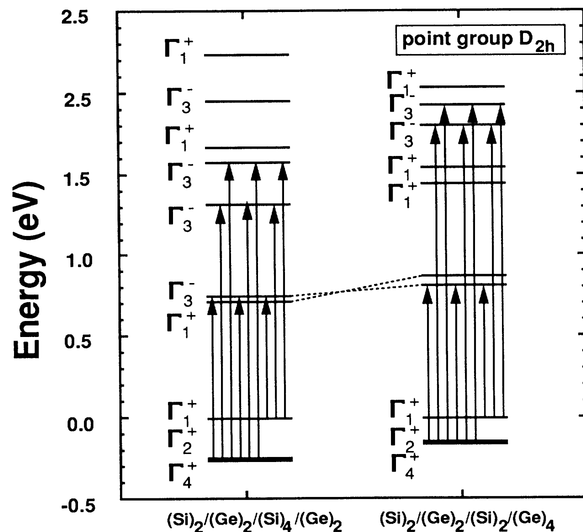

FIG. 10. Energy-level diagrams at the Γ point for $(Si)_2/(Ge)_2/(Si)_4/(Ge)_2$ and $(Si)_2/(Ge)_2/(Si)_2/(Ge)_4$ on the Ge(001) substrate. The point-group symmetry at the Γ point for these modulated superlattices is D_{2h}. The lowest three levels belong to the valence band and the highest seven levels to the conduction band. Optical transition is allowed between states connected by an arrow. For simplicity, the lowest three optical transitions between states are indicated.

In Fig. 12(a), as the width of the potential well is narrow, the amplitude of the antisymmetric wave function cannot exceed that of the symmetric wave function within the potential well. Therefore, the lowest state has a larger weight at the potential well (Si region) than the second-lowest state. In Fig. 12(b), the same argument is applicable to the Ge region. This, in turn, implies that the second-lowest state has a larger weight at the potential well (Si region) than the lowest state. These two cases may correspond to Fig. 11(b).

In Fig. 12(c), mirror symmetry points are located at the centers of the potential hills (Ge region). Therefore, the second-lowest state has reduced weight in the Ge region and thereby has a larger weight at the Si region than at the lowest state. In Fig. 12(d), mirror symmetry points are located at the centers of the potential wells (Si region). Therefore, the second-lowest state has nodes in the Si region. Clearly, the lowest state has a larger weight at the Si region than the second-lowest state. These latter two cases may correspond to 4′ and 6′ in Fig. 11(a).

The above arguments seem to explain the trend in Figs. 11(a) and 11(b) successfully. However, we must note that in the real Si/Ge superlattices, both of Γ_1^+ and Γ_3^- (or Γ_2^-) states have rather complicated nodal structures not only in the stacking direction but also within each atomic layer. We cannot assign the Γ_1^+ state to the symmetric ground state or the Γ_3^- state to the antisymmetric excited state. Although it is not clear at present how the argument of Fig. 12 is related to our realistic cases, such a simple argument is suggestive for the trends in Fig. 11.

D. $(Si)_4/(Ge)_4$ on Si substrate: Interface alloying effects

The $(Si)_4/(Ge)_4$ superlattices were grown on the Si substrate and studied by the electrorefrectance spectroscopy.[1,18] New optical transitions at the Γ point due to the superlattice structure were found at 0.76, 1.25, and 1.70 eV. This experimental result stimulated many theoretical calculations because the experiments seemed to suggest that this superlattice might be a direct-band-gap material.[6–13]

TABLE V. The estimated energy separations for the lowest and the second-lowest conduction-band states of the modulated superlattices on the Ge(001) substrate. The values in the parentheses are for $(Si)_{2m}/(Ge)_{10-2m}$ with the same component. ξ is the distortion parameter as defined in Fig. 6. The energy separations of our first-principles calculations are also shown for comparison. The first-order perturbation theory accounts well for the trend.

Modulated superlattices	First-order perturbation theory Analytic form	ξ	Energy separation (eV)		First-principles calculations Energy separation (eV)	
$[(Si)_1/(Ge)_4]_2$	$-\frac{8}{5}\times 0.186$	0.99	−0.149	(−0.042)	−0.248	(−0.270)
$[(Si)_2/(Ge)_3]_2$	$-\frac{8}{5}\sin\frac{\pi}{10}\times 0.186$	0.97	−0.093	(0.070)	−0.172	(0.088)
$[(Si)_3/(Ge)_2]_2$	$-\frac{8}{5}\sin\frac{\pi}{10}\times 0.191$	0.96	0.094	(−0.071)	0.029	(−0.101)
$[(Si)_4/(Ge)_1]_2$	$-\frac{4}{5}\sin\frac{\pi}{10}\times 0.194$	0.94	0.155	(0.044)	0.205	(0.024)
$(Si)_2/(Ge)_2/(Si)_4/(Ge)_2$	$\frac{4}{5}\left[1-\sin\left[\frac{3\pi}{10}\right]\right]\times 0.191$	0.96	0.029	(−0.077)	0.034	(−0.101)
$(Si)_2/(Ge)_2/(Si)_2/(Ge)_4$	$-\frac{4}{5}\left[1-\sin\left[\frac{3\pi}{10}\right]\right]\times 0.189$	0.97	−0.028	(0.075)	−0.060	(0.088)

In Fig. 13(a), the band dispersion of $(Si)_4/(Ge)_4$ with ideal interfaces grown on the Si substrate is shown. The conduction-band bottom is located near the X point along the transverse Δ line. The energy gap is 0.88 eV and its transition type is indirect. The corresponding value by Hybertsen and Schlüter is 0.85 eV.[7] Based on the analysis of the photon-energy dependence of the absorption intensity, Hybertsen *et al.*[19] argued that the transition near 0.8 eV (0.78 eV in their work rather than 0.76 eV) would be indirect. However, they also pointed out that the observed intensity is much stronger than expected for an indirect transition. Therefore, the nature of this transition is still an open question.

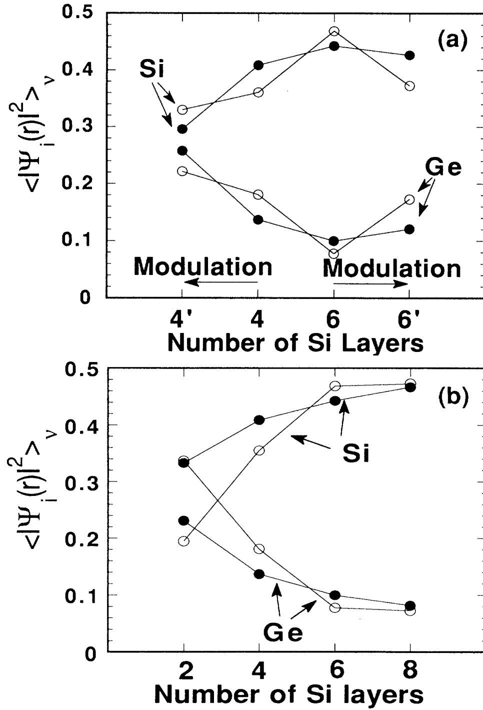

FIG. 11. Integral of the wave function squared over the Si(Ge) atomic spheres in a unit cell for the (4/6), (6/4), and the corresponding modulated (2/2/4/2) and (2/2/2/4) is shown in (a). Solid circles are for the lowest conduction-band state at the Γ point and open circles for the second-lowest conduction-band state. The results for $(Si)_{2m}/(Ge)_{10-2m}$ are also shown in (b) for comparison.

Here, we propose an interpretation to remove the discrepancy by considering the alloying effects at the interfaces.[12] In the real superlattices the interfaces are not perfectly sharp and, in fact, some experiments show the existence of ordering phenomena in the actual heterointerfaces.[30] In order to see the effects of ordering phenomena on the electronic structures of superlattices, we simulated the alloying at the heterointerfaces as shown in Fig. 14. We introduced an artificial two-layer ordered Si-Ge compound into every Si-Ge interface. This model of heterointerface diffusion is a hybrid of the Ourmazd-Bean[31] and the Ciraci-Batra[10] models for the (111) natural superlattice for Si-Ge alloys grown on the Si substrate which fulfill the extinction rule for the observed superlattice diffraction spots.[30–32]

Figure 13(b) shows the $E-\mathbf{k}$ curve of $(Si)_4/(Ge)_4$ with interdiffused interfaces mentioned above. The conduction-band bottom is located nearly at the same point as in Fig. 13(a) with an indirect-band gap of 0.84 eV. Because of the additional periodicity along the (110) direction, folded bands are also shown. Along the Γ-Z direction, the minimum in the conduction band is at the Γ point in this case whereas it is at the Z point in Fig. 13(a). This difference may be due to some subtle effects of the ordering phenomena and the chemical effects at the interface.

While the symmetry at the Γ point is D_{2h} for the ideal $(Si)_4/(Ge)_4$ superlattice, the one for the interdiffused case is C_{2h}. The energy-level diagrams at the Γ point are shown in Fig. 15 for the two cases. Between the levels connected by vertical arrows, the dipole transition is allowed.

In Fig. 16, the experimentally observed energy levels and optically allowed transition levels of our calculations at the Γ point are illustrated. The 0.76-, 1.25-, and 1.70-eV levels are experimentally observed for this system.[1,18] In the case of the ideal interface, our calculated results indicate that theoretical energy levels appear at 1.27, 1.28, 1.66, and 1.68 eV, which are close to the observed levels. However, there is no level corresponding to the observed 0.76-eV level. The lowest optical transition energy is 1.04 eV for the interdiffused model. The energy of the lowest transition for the alloying model becomes lower than that of the ideal case by 0.23 eV but is still higher than the observed level by 0.3 eV. According to our calculations for Si-Ge superlattices, the change of the substrate from Si to Ge causes lowering of the conduction bands at the Γ point. Therefore, the remaining discrepancy may be partly removed by partial relaxation of the strain in the actual superlattices.

In Table VI, we show the magnitude of optical transition probability for $(Si)_4/(Ge)_4$ with both the interdiffused

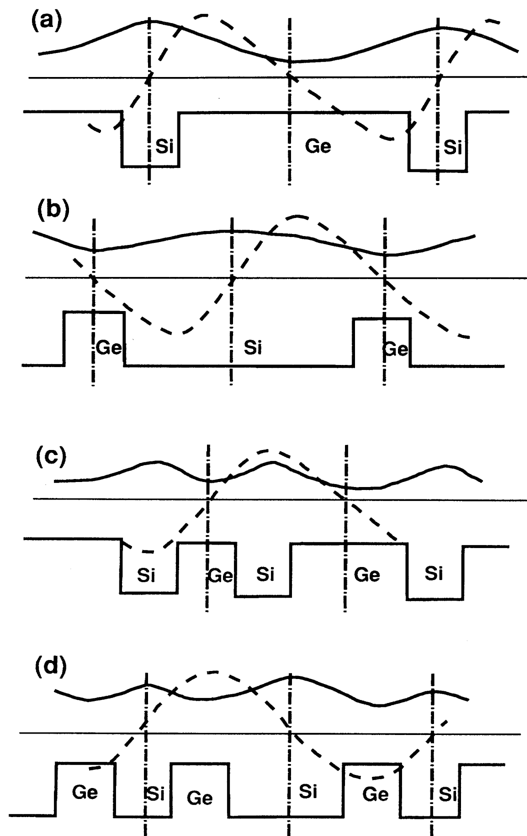

FIG. 12. A simple one-dimensional model to interpret the results of Fig. 11. (a)–(d) simulate (2/8), (8/2), (2/2/2/4), and (2/2/4/2). Deeper potential regions correspond to Si layers and shallower potential regions to Ge layers. The vertical dot-dashed lines denote the positions with regard to which the system has mirror symmetry. The lowest two states at the Γ point are considered. The lowest-state wave function (solid line) is symmetric, while the second-lowest state one (dashed line) is antisymmetric with respect to mirror symmetry.

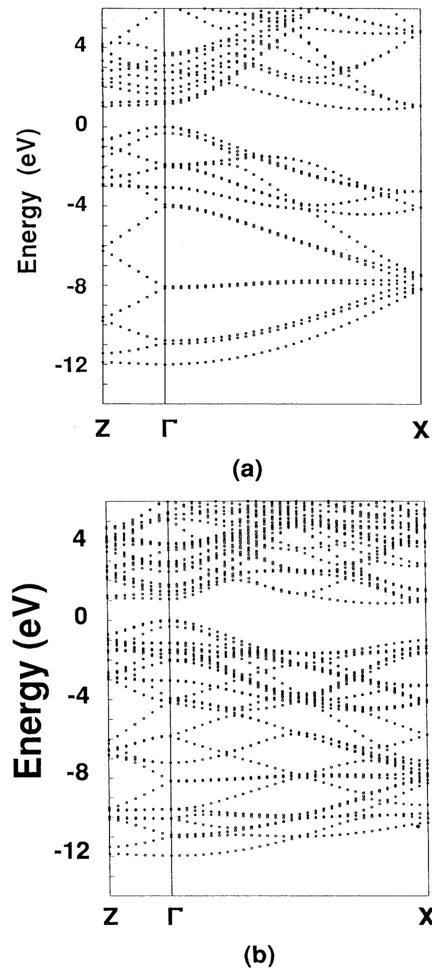

FIG. 13. The E-$\mathbf{k}$ curves along the Z-Γ-X direction for the $(Si)_4/(Ge)_4$ superlattice on the Si(001) substrate (a) for the ideal interface of Fig. 14(a) and (b) for the interdiffused interface of Fig. 14(b).

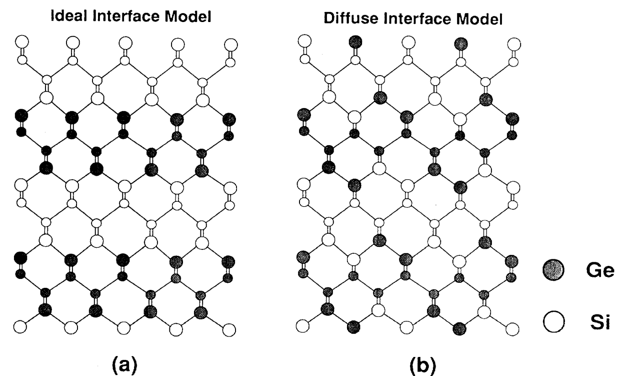

FIG. 14. The positions of the atoms in the $(Si)_4/(Ge)_4$ superlattice with the ideal interfaces are shown in (a). The model structure for the $(Si)_4/(Ge)_4$ superlattice with the interdiffused interfaces is shown in (b). An artificial two-layer ordered Si-Ge compound is introduced into every Si-Ge interface in this model structure.

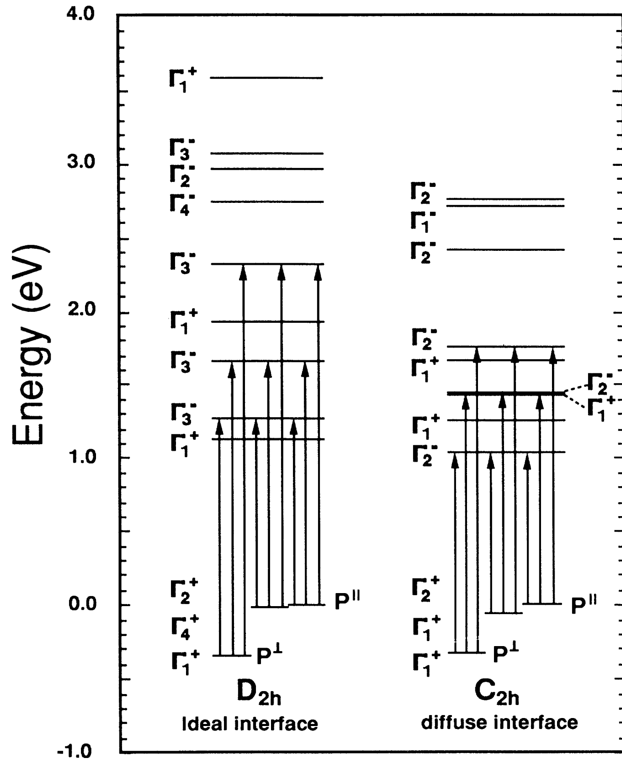

FIG. 15. Energy-level diagrams at the Γ point for $(Si)_4/(Ge)_4$ on the Si(001) substrate (a) for the ideal interfaces and (b) for the interdiffused interfaces. The optical transitions are allowed between the states connected by arrows. Some higher-energy optical transitions are not indicated for simplicity.

and the ideal interfaces. By introducing the alloying effects into the interface, the optical transition probability becomes larger than that of the ideal case by one order of magnitude. It should be noted that there appear three additional energy levels compared to the ideal superlattice.

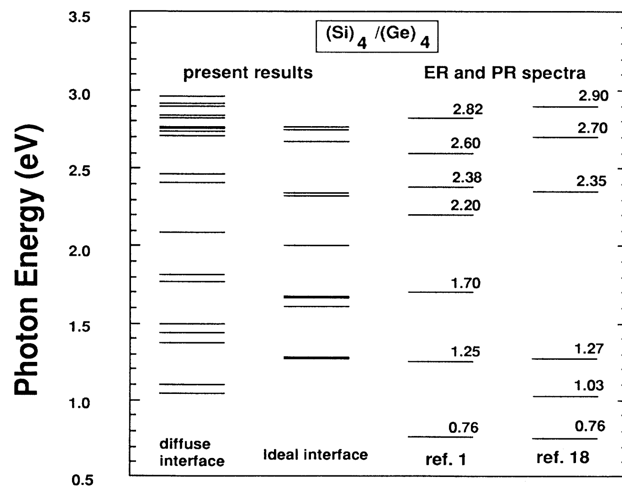

FIG. 16. Optically allowed transition levels of our calculations at the Γ point are illustrated. The experimentally observed energy levels are also shown for comparison.

The light polarization of the transition between Γ_{v2} (Γ_{v3}) and conduction bands shows the partial mixing of the P_x and P_y polarizations. This is probably due to the effects of the long-range order perpendicular to the growth direction.

Our proposal here is that unsolved 0.76-eV transition for $(Si)_4/(Ge)_4$ may be understood by considering the effects of the interface alloying and the strain effects due to the partial relaxation of the substrate. Although our model is one of the possible candidates for the real interface diffusions, it improves the situation to some extent. Considering that the perfect interface case accounts well for the transitions except for the near 0.8-eV transition, the real interface may be a mixture of the perfect interface and some alloyed one.

IV. CONCLUSIONS

We have investigated the electronic structures of Si-Ge strained layer superlattices based on the first-principles calculations. By implementing SIC into the orbital-defining equations in the LMTO method, the energy gaps for typical semiconductors are well described. As for the band offset of Si/Ge systems, our calculated values are in good agreement with the experimental ones.

By using our LMTO-SIC method, we have studied the electronic structures of various kinds of Si-Ge superlattices and their optical properties. As is first pointed out by Hybertsen, Friedel, and Schlüter,[9] based on the empirical pseudopotential method, we have confirmed that the ten-layer periodicity is a suitable condition to make the Si-Ge superlattices direct-band-gap type as long as the strain caused by the substrate moves the energy along the transverse Δ line upward. We have found an alternating change of the allowed and the forbidden optical transitions between the lowest conduction-band and the highest valence-band levels. These are analyzed successfully by the first-order perturbation theory.

We have proposed Si-Ge superlattice structures by modulating the layer construction of $(Si)_m/(Ge)_{10-m}$ into $(Si)_p/(Ge)_q/(Si)_r/(Ge)_s$ $(p+q+r+s=10)$. Our calculated results indicate that the band structures of $(Si)_3/(Ge)_2$, $(Si)_2/(Ge)_3$, $(Si)_2/(Ge)_2/(Si)_4/(Ge)_2$, and $(Si)_2/(Ge)_2/(Si)_2/(Ge)_4$ grown on the Ge substrate are of the direct-band-gap type. We have analyzed the symmetry property at the Γ point for these superlattices and again found the alternating change of allowed and forbidden transitions. These behaviors are also explained by the first-order perturbation theory. As for the optical transitions, the intensity increases by introducing modulations into the superlattices. We have found an interesting aspect of the wave-function confinement for the lowest two conduction-band states. Although we have not completely understood the basic mechanism, we have pointed out a possible similar phenomenon in a simple one-dimensional model.

Finally, we have commented on the discrepancy between the theory and experiment with regard to the 0.76-eV transition for the $(Si)_4/(Ge)_4$ superlattice grown on the Si substrate. By noting that the real superlattice will have diffuse interfaces, we introduced a particular

TABLE VI. Calculated dipole matrix elements $|\langle i|P|f\rangle|^2$ and transition energies ΔE in $(Si)_4/(Ge)_4$ superlattices on the Si substrate for the ideal and the interdiffused interface models of Fig. 14. Energy differences are in eV. The direction of polarization is denoted by P_x, P_y, or P_z. The matrix elements are normalized so that the strong transition of bulk character is unity.

$\langle i\|$		Γ_{v_1}			Γ_{v_2}			Γ_{v_3}	
$\|f\rangle$	ΔE	$\|\langle i\|P\|f\rangle\|^2$		ΔE	$\|\langle i\|P\|f\rangle\|^2$		ΔE	$\|\langle i\|P\|f\rangle\|^2$	
				D_{2h} ideal interface					
Γ_{c_2}	1.27	0.0032	P_x	1.28	0.0061	P_y	1.61	0.0056	P_z
Γ_{c_3}	1.66	0.0042	P_x	1.68	0.0529	P_y	2.01	0.0197	P_z
Γ_{c_5}	2.33	1.0	P_x	2.34	1.0	P_y	2.67	1.0	P_z
				C_{2h} interdiffused interface					
Γ_{c_1}	1.04	0.0573	P_y	1.10	0.0532	P_x,P_z	1.37	0.0567	P_z,P_x
Γ_{c_4}	1.44	0.0495	P_y	1.49	0.0673	P_x,P_z	1.77	0.0645	P_z,P_x
Γ_{c_6}	1.77	0.0914	P_y	1.82	0.0287	P_x,P_z	2.09	0.0624	P_z,P_x
Γ_{c_7}	2.41	1.0	P_y	2.46	1.0	P_x,P_z	2.74	1.0	P_z,P_x

type of Si-Ge compound into each interface. Although the calculated electronic structure for this interdiffused superlattice is not perfectly consistent with the experimental data, the alloying effect removes the discrepancy to some extent. We pointed out also that partial relaxation of the strain in the superlattice will reduce the discrepancy further.

ACKNOWLEDGMENTS

This work was partially supported by a Grant-in-Aid for Scientific Research on Priority Areas from the Ministry of Education, Science and Culture. Numerical calculations were performed mostly at Fujitsu Laboratories and partly at the Computer Center of Institute for Molecular Science.

[1]T. P. Pearsall, J. Bevk, L. C. Feldman, J. M. Bonar, J. P. Mannaerts, and A. Ourmazd, Phys. Rev. Lett. **58**, 729 (1987).

[2]T. P. Pearsall, J. Bevk, J. C. Bean, J. M. Bonar, J. P. Mannaerts, and A. Ourmazd, Phys. Rev. B **39**, 3741 (1989).

[3]R. Zachai, K. Eberl, G. Abstreiter, E. Kasper, and H. Kibble, Phys. Rev. Lett. **64**, 1055 (1990).

[4]T. P. Pearsall, J. M. Vandenberg, R. Hull, and J. M. Bonar, Phys. Rev. Lett. **63**, 2104 (1989).

[5]U. Gnutzman and K. Clausecker, Appl. Phys. **3**, 9 (1974).

[6]S. Froyen, D. M. Wood, and A. Zunger, Phys. Rev. B **36**, 4547 (1987); **37**, 6893 (1988).

[7]M. S. Hybertsen and M. Schlüter, Phys. Rev. B **36**, 9683 (1987).

[8]S. Satpathy, R. M. Martin, and C. G. Van de Walle, Phys. Rev. B **38**, 13 237 (1988).

[9]M. S. Hybertsen, P. Friedel, and M. Schlüter, in *Proceedings of the 19th International Conference on the Physics of Semiconductors,* edited by W. Zawadzki (Polish Academy of Sciences, Warsaw, Poland, 1988), p. 491.

[10]S. Ciraci and I. P. Batra, Phys. Rev. B **38**, 1835 (1988).

[11]M. Ikeda, T. Oghuchi, and K. Terakura, in *Proceedings of the 19th International Conference on the Physics of Semiconductors* (Ref. 9), p. 495.

[12]M. Ikeda, K. Terakura, and T. Oguchi, in *Proceedings of the 20th International Conference on the Physics of Semiconductors,* edited by E. M. Anastassakis and J. D. Joannopoulos (World Scientific, Thessaloniki, Greece, 1990), p. 889.

[13]U. Schmid, N. E. Chiristensen, M. Alouani, and M. Cardona, Phys. Rev. B **43**, 14 597 (1991).

[14]O. K. Andersen, Phys. Rev. B **12**, 3060 (1975).

[15]As a recent review, see R. O. Jones and O. Gunnarsson, Rev. Mod. Phys. **61**, 689 (1989).

[16]N. Hamada and S. Ohnishi, Phys. Rev. B **34**, 9042 (1986).

[17]M. Ikeda, K. Terakura, and T. Oguchi, Phys. Rev. B **45**, 1496 (1992).

[18]K. Asami, K. Miki, K. Sakamoto, T. Sakamoto, and S. Gonda, Jpn. J. Appl. Phys. **29**, L381 (1990).

[19]M. S. Hybertsen, M. Schlüter, R. People, S. A. Jackson, D. V. Lang, T. P. Peasall, J. C. Bean, J. M. Vandenberg, and J. Bevk, Phys. Rev. B **37**, 10 195 (1988).

[20]R. M. Martin, Phys. Rev. B **1**, 4005 (1970).

[21]H. Oyanagi, in *Extended Abstracts of the 19th Conference on Solid State Devices and Materials,* edited by S. Furukawa (Japan Society of Applied Physics, Tokyo, 1987), p. 487.

[22]N. Hamada, M. Hwang, and A. J. Freeman, Phys. Rev. B **41**, 3620 (1990).

[23]*Zahlenwerte und Funktionen aus Naturwissen-schaften und Technik,* edited by O. Madelung, M. Schulz, and H. Weiss, Landolt-Börnstein, New Series, Group 3, Vol. 17, Pt. a (Springer, Berlin, 1982).

[24]M. S. Hybertsen and S. G. Louie, Phys. Rev. Lett. **55**, 1418 (1985); Phys. Rev. B **32**, 7005 (1986); **34**, 5390 (1986).

[25]G. P. Schwartz, M. S. Hybertsen, J. Bevk, R. G. Nuzzo, J. P. Manaerts, and G. J. Gualtieri, Phys. Rev. B **39**, 1235 (1989).

[26]J. Tersoff and C. G. Van de Walle, Phys. Rev. Lett. **59**, 946 (1987).

[27]C. G. Van de Walle and R. M. Martin, Phys. Rev. B **34**, 5621 (1986).

[28]P. Friedel, M. S. Hybertsen, and M. Schlüter, Phys. Rev. B **39**, 7974 (1989).

[29]C. J. Bradley and A. P. Cracknell, *The Mathematical Theory of Symmetry in Solids* (Clarendon, Oxford, 1972), pp. 58 and 59.

[30]M. Müller, H.-U. Nissen, M. Ospelt, and H. von Känel, Phys. Rev. Lett. **63**, 1819 (1989).

[31]A. Ourmazd and J. C. Bean, Phys. Rev. Lett. **55**, 765 (1985).

[32]F. K. LeGoues, V. P. Kesan, and S. S. Iyer, Phys. Rev. Lett. **64**, 40 (1990).